

# Nonlinear Peculiar-Velocity Analysis and PCA

Avishai Dekel<sup>1</sup>, Amiram Eldar<sup>1</sup>, Lior Silberman<sup>1</sup>, and Idit Zehavi<sup>2</sup>

<sup>1</sup> Racah Institute of Physics, The Hebrew University, Jerusalem 91904, Israel

<sup>2</sup> NASA/Fermilab Astrophysics Group, FNAL, Box 500, Batavia, IL 60510, USA

**Abstract.** We allow for nonlinear effects in the likelihood analysis of peculiar velocities, and obtain  $\sim 35\%$ -lower values for the cosmological density parameter and for the amplitude of mass-density fluctuations. The power spectrum in the linear regime is assumed to be of the flat  $\Lambda$ CDM model ( $h = 0.65$ ,  $n = 1$ ) with only  $\Omega_m$  free. Since the likelihood is driven by the nonlinear regime, we “break” the power spectrum at  $k_b \sim 0.2 (h^{-1}\text{Mpc})^{-1}$  and fit a two-parameter power-law at  $k > k_b$ . This allows for an unbiased fit in the linear regime. Tests using improved mock catalogs demonstrate a reduced bias and a better fit. We find for the Mark III and SFI data  $\Omega_m = 0.35 \pm 0.09$  with  $\sigma_8 \Omega_m^{0.6} = 0.55 \pm 0.10$  (90% errors). When allowing deviations from  $\Lambda$ CDM, we find an indication for a wiggle in the power spectrum in the form of an excess near  $k \sim 0.05$  and a deficiency at  $k \sim 0.1 (h^{-1}\text{Mpc})^{-1}$  — a “cold flow” which may be related to a feature indicated from redshift surveys and the second peak in the CMB anisotropy. A  $\chi^2$  test applied to principal modes demonstrates that the nonlinear procedure improves the goodness of fit. The Principal Component Analysis (PCA) helps identifying spatial features of the data and fine-tuning the theoretical and error models. We address the potential for optimal data compression using PCA.

## 1 Introduction

When the large-scale density fluctuations are assumed to be Gaussian, they are fully characterized by their power spectrum  $P(k)$ , which is directly related to cosmological parameters that we wish to estimate. The  $P(k)$  as estimated from redshift surveys is contaminated by unknown “galaxy biasing”, redshift distortions, triple-value zones and the nonlinearity of the density field. It is therefore advantageous to estimate the mass-density  $P(k)$  directly from dynamical data such as peculiar velocities (PVs), which avoid biasing and suffers from weaker nonlinear effects. The  $P(k)$  is evaluated here via a likelihood analysis of the individual PVs, not via a reconstruction method like POTENT (Dekel *et al.* 1999). The simplifying assumptions made in turn are that the PVs are drawn from a Gaussian random field, the velocity correlations can be derived from the density  $P(k)$  using linear theory, and the errors are Gaussian. The method assumes as prior a parametric functional form for the  $P(k)$ , which allows cosmological parameter estimation.

We use two PV catalogs. The Mark III (M3) catalog (Willick *et al.* 1997) contains  $\sim 3000$  galaxies within  $\sim 70 h^{-1}\text{Mpc}$  from several datasets of spirals and ellipticals with distances inferred by the Tully-Fisher (TF) and  $D_n - \sigma$

methods. The SFI catalog (Haynes *et al.* 1999) consists of  $\sim 1300$  late-type spirals with I-band TF distances from two datasets. The catalogs cover a similar volume, with the M3 sampling denser nearby and sparser at large distances. The errors are  $\sim 15 - 21\%$  of the distance. In M3, the galaxies were grouped into  $\sim 1200$  objects and then corrected for Malmquist bias. The SFI data were corrected for biases as in Freudling *et al.* (1999, F99).

In Zaroubi *et al.* (1997, Z97) and F99, we applied a likelihood analysis with a linear  $P(k)$  model on all scales, taken from the family of COBE-normalized CDM models. The free parameters were  $\Omega_m$ ,  $n$ , and  $h$ . The two datasets yielded a high  $P(k)$ , defining a surface in parameter space:  $\Omega_m h_{65}^{1.3} n^2 \simeq 0.54 \pm 0.10$  (flat universe, no tensor fluctuations). Correspondingly,  $\sigma_8 \Omega_m^{0.6} \simeq 0.84 \pm 0.12$ . These seemed to be consistent with the  $2\sigma$  lower bounds of  $\Omega_m > 0.3$  obtained from PVs by other biasing-free methods (Nusser & Dekel 1993; Dekel & Rees 1994; Bernardeau *et al.* 1995), but they imply higher values than obtained from other estimators, e.g. based on cluster abundance (White, Efstathiou & Frenk 1993; Eke *et al.* 1998).

The method has been tested using mock catalogs drawn from an N-body simulation of limited resolution. We therefore generated new mock catalogs based on simulations of higher resolution, which reveal a significant bias in the linear analysis. The fit is driven by the small scales, because close pairs tend to consist of nearby galaxies with small errors, and therefore weak nonlinear effects on small scales may bias the results. We improve the analysis by adding free parameters that allow independent matching of the nonlinear behavior and thus an unbiased determination of the linear part of the spectrum and the associated cosmological parameters. We then investigate the  $P(k)$  independent of a specific cosmological model, by allowing as free parameters the actual values of  $P(k)$  in finite intervals of  $k$  (also in Zehavi & Knox, in preparation).

The likelihood analysis provides only relative likelihoods of the parameters, not an absolute goodness of fit (GOF). An indication for a problem in the GOF of the linear analysis came from a  $\chi^2$  estimate in modes (Hoffman & Zaroubi 2000). It seems to be associated with a problem noticed earlier by F99, of a spatial gradient in the obtained value of  $\Omega_m$ . We therefore develop a method based on  $\chi^2$  in PCA as a tool for evaluating the GOF in our new procedure compared to the old one.

In §2 we describe the method. In §3 we test and calibrate it using mock catalogs. In §4 we present the resultant  $P(k)$  and  $\Omega_m$  for  $\Lambda$ CDM. In §5 we detect hints for deviations from this model. In §6 we describe the PCA. In §7 we evaluate GOF via  $\chi^2$  in modes of PCA. In §8 we conclude.

## 2 Method

As explained in Z97 and F99, the goal is to estimate the density  $P(k)$  from PVs by finding maximum likelihood values for parameters of an assumed

model  $P(k)$ . Under the assumption that the underlying velocities and the observational errors are independent Gaussian random fields, the likelihood is

$$\mathcal{L} = \frac{1}{[(2\pi)^n \det(C)]^{1/2}} \exp\left(-\frac{1}{2} \sum_{i,j} u_i C_{ij}^{-1} u_j\right), \quad (1)$$

where  $\{u_i\}_{i=1}^n$  are the observed PVs at locations  $\{\mathbf{r}_i\}$ , and  $C$  is their correlation matrix. Expressing each data point as signal plus noise,  $u_i = s_i + n_i$ ,

$$C_{ij} \equiv \langle u_i u_j \rangle = \langle s_i s_j \rangle + \langle n_i n_j \rangle \equiv S_{ij} + N_{ij}. \quad (2)$$

$S$  is the correlation matrix of the signal, calculated from the  $P(k)$  model at  $\mathbf{r}_i$ , and  $N$  is the error matrix, assumed diagonal because the errors of the objects are uncorrelated. For a given  $P(k)$ ,  $S_{ij}$  are calculated via the parallel and perpendicular velocity correlation functions,  $\Psi_{\parallel}$  and  $\Psi_{\perp}$ ,

$$S_{ij} = \Psi_{\perp}(r) \sin \theta_i \sin \theta_j + \Psi_{\parallel}(r) \cos \theta_i \cos \theta_j, \quad (3)$$

where  $r = |\mathbf{r}| = |\mathbf{r}_j - \mathbf{r}_i|$  and the angles are defined by  $\theta_i = \hat{\mathbf{r}}_i \cdot \hat{\mathbf{r}}$  (Górski 1988; Groth, Juszkiewicz & Ostriker 1989). In linear theory,

$$\Psi_{\perp,\parallel}(r) = \frac{H_0^2 f^2(\Omega_m)}{2\pi^2} \int_0^{\infty} P(k) K_{\perp,\parallel}(kr) dk, \quad (4)$$

where  $K_{\perp}(x) = j_1(x)/x$  and  $K_{\parallel}(x) = j_0 - 2j_1(x)/x$ , with  $j_l(x)$  the spherical Bessel function of order  $l$ . The  $\Omega_m$  dependence enters as usual via  $f(\Omega_m) \simeq \Omega_m^{0.6}$ .

For each choice of parameters,  $C$  is computed, inverted, and substituted in Eq. (1). Exploring parameter space, we find the parameters that maximize the likelihood. The main computational effort is the inversion of  $C$  in each evaluation of the likelihood. It is an  $n \times n$  matrix, where currently  $n \sim 10^3$ , but when  $n$  increases soon, a procedure for data compression will be required (see §6).

The measurement errors add in quadrature to the  $P(k)$  and thus propagate into a systematic uncertainty. Z97 used *a priori* estimates of the errors, while F99 incorporated the errors into the likelihood analysis via an error model with free parameters. They found errors within 5% of the *a priori* estimates, thus allowing the use of the *a priori* estimates here. Relative confidence levels are estimated by approximating  $-2\ln\mathcal{L}$  as a  $\chi^2$  distribution with respect to the model parameters.

In the linear regime, we use as prior the parametric form based on the general CDM model,  $P(k) = A_c(\Omega_m, \Omega_{\Lambda}, n) T^2(\Omega_m, \Omega_b, h; k) k^n$ , where  $A_c$  is the normalization factor and  $T(k)$  is the CDM transfer function proposed by Sugiyama (1995). We restrict ourselves in the present paper to flat cosmology with a cosmological constant ( $\Omega_m + \Omega_{\Lambda} = 1$ ), a scale-invariant power spectrum on large scales ( $n = 1$ ), and a Hubble constant  $h = 0.65$ .

The baryonic density is set to be  $\Omega_b = 0.024h^{-2}$  (Tytler, Fan & Burles 1996), and the amplitude  $A_c$  is fixed by the COBE 4-year data (Hinshaw *et al.* 1996; Górski *et al.* 1998). The analysis has been repeated with a later estimate of  $\Omega_b = 0.019h^{-2}$  (Burles *et al.* 1999) and an alternative COBE normalization (Bunn & White 1997), with variations  $< 2\%$  due to these changes.

An accurate nonlinear correction to the linear *velocity* power spectrum could have been very useful in avoiding the bias associated with the linear analysis, but such a correction is not yet available. An empirical approximation does exist for the nonlinear correction to the *density*  $P(k)$  (Peacock & Dodds 1996, PD), but the generalization to a velocity correction is not straightforward. Here, we detach the nonlinear regime from the linear regime by a “break” in the  $P(k)$  at a wavenumber  $k_b$ . We then assume the  $\Lambda$ CDM shape at  $k < k_b$ , determined by  $\Omega_m$ , and allow an almost arbitrary power law with two free parameters to fit the data at  $k > k_b$ . This “feeds the nonlinear monster” while the linear part of the spectrum, and the associated cosmological parameters, are freed to be determined unbiased.

### 3 Testing with Mock Catalogs

We test the method using mock catalogs based on cosmological simulations in which the “true” cosmological parameters and linear  $P(k)$  are fully known *a priori*, and where nonlinear effects are simulated with adequate accuracy. We use the unconstrained “GIF” simulation (Kauffmann *et al.* 1999a) of the flat  $\Lambda$ CDM cosmology with  $\Omega_m = 0.3$ . The initial fluctuations were Gaussian, adiabatic and scale-invariant,  $n = 1$ . The  $P(k)$  shape parameter was  $\Gamma = \Omega_m h = 0.21$  (namely  $h = 0.7$ ) and the amplitude is such that  $\sigma_8 = 0.9$ , consistent with both the present cluster abundance and COBE’s measurements on large scales. The  $N$ -body code is a version of the adaptive particle-particle particle-mesh (AP<sup>3</sup>M) Hydra code developed as part of the VIRGO supercomputing project (Jenkins *et al.* 1998). The simulation has  $256^3$  particles and  $512^3$  cells, and a gravitational softening length of  $30 h^{-1} \text{kpc}$ , inside a box of side  $141.3 h^{-1} \text{Mpc}$ . Dark-matter halos were identified using a friends-of-friends algorithm with a linking length of 0.2 and a minimum of 10 particles per halo was imposed. Luminous galaxies were planted in the halos based on a semi-analytic scheme (Kauffmann *et al.* 1999a, 1999b). We assigned to each galaxy a linewidth based on the TF relation and the scatter assumed in Kolatt *et al.* (1996). We then generated 10 mock catalogs which resemble the M3 catalog, with random distance errors and random sampling. The mock data were grouped and corrected for Malmquist biases exactly as in the real data.

To study how the method performs in the presence of nonlinear effects, we produced a suite of 10 sets of 10 mock catalogs each, spanning a range of degree of nonlinearity, created by varying the criterion for the exclusion of cluster galaxies. Galaxies were excluded if they lie within a distance  $r_c$

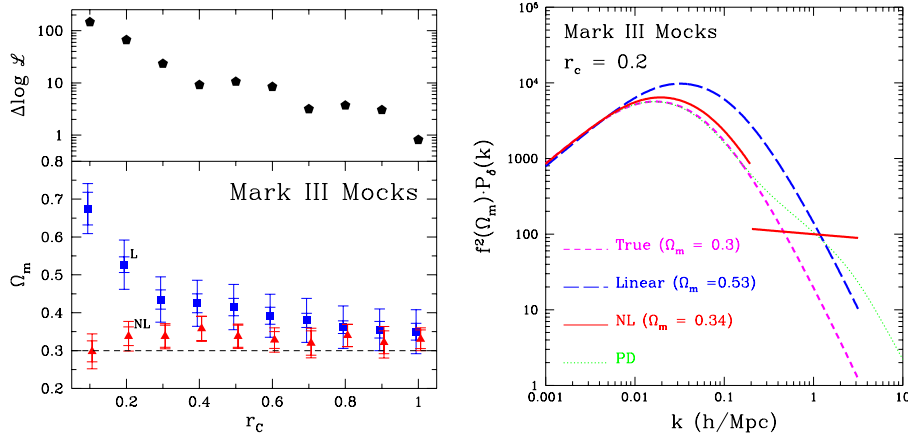


**Fig. 1.** Testing the method. **Left:** *Bottom:* the recovered  $\Omega_m$  as a function of the degree of linearity of the dataset,  $r_c$ . Each symbol marks the average over 10 mock M3 catalogs, and the inner and outer error bars mark the scatter and 90% likelihood uncertainty. The squares are the results of the linear analysis; they show a bias that increases with the degree of nonlinearity. The triangles are the results of the broken- $\Lambda$ CDM  $P(k)$ ; the bias is drastically reduced. *Top:* the corresponding improvement in  $\log \mathcal{L}$  for the nonlinear versus linear analysis. **Right:** Mean power spectra recovered from the M3 mock catalogs of  $r_c = 0.2$ . The target is the true linear  $P(k)$ . The biased linear result is shown. The result from the nonlinear analysis with  $k_b = 0.2 (h^{-1}\text{Mpc})^{-1}$  is marked “NL”. The  $P(k)$  is in units of  $(h^{-1}\text{Mpc})^3$ .

from the cluster center. The “linearity parameter”  $r_c$  is measured in units of  $3.5 h^{-1}\text{Mpc}$  and  $1.5 h^{-1}\text{Mpc}$  for spirals and ellipticals respectively, and it ranges from  $r_c = 0.1$  to 1 in steps of 0.1. The likelihood analysis has been applied to each of the  $10 \times 10$  mock M3 catalogs. The recovered values of  $\Omega_m$  are shown in Figure 1 (left). The “true” target value is the  $\Omega_m = 0.3$  of the simulation.

We first apply the purely linear analysis, with the linear  $\Lambda$ CDM power spectrum at all scales, and with  $\Omega_m$  as the only free parameter. We see that the linear likelihood analysis systematically overestimates the value of  $\Omega_m$ . As the data become more nonlinear, the recovered value of  $\Omega_m$  becomes higher, and the bias more significant. Next, we apply the improved procedure, allowing for a break in the  $P(k)$  at  $k_b = 0.2 (h^{-1}\text{Mpc})^{-1}$  and additional free parameters in the nonlinear regime. We see that the bias is practically removed for all levels of nonlinearity. The figure also shows the corresponding improvement in  $\log \mathcal{L}$  when the linear analysis is replaced with the nonlinear analysis. Figure 1 shows the corresponding power spectra from the M3 mock catalogs of linearity  $r_c = 0.2$ .

Our conclusion from the above test using the mock catalogs is that, in the presence of significant nonlinear effects in the data, the purely linear

likelihood analysis might yield a biased estimate of  $P(k)$  and  $\Omega_m$ . The broken- $P(k)$  analysis successfully eliminates the dependence of the results on the nonlinear effects and practically corrects the bias in the results.

#### 4 Broken $\Lambda$ CDM: the Value of $\Omega_m$

We now analyze the real data. Our  $\Lambda$ CDM model is restricted again to a flat universe with  $h = 0.65$ ,  $\Omega_b h^2 = 0.02$  and  $n = 1$ , leaving only one cosmological parameter free,  $\Omega_m$ . Unlike the mock tests, we now do not know that  $\Lambda$ CDM is the right model or that the values of the fixed parameters are accurate. Figure 2 shows the resultant power spectra. The linear analysis yields a high  $P(k)$  amplitude and a high value of  $k_{\text{peak}}$ , corresponding to  $\Omega_m = 0.56 \pm 0.04$  and  $\Omega_m = 0.51 \pm 0.05$  for M3 and SFI (90% errors), consistent with Z97 and F99 for the fixed values of  $h$  and  $n$  quoted above. The nonlinear analysis yields a shift of  $k_{\text{peak}}$  towards lower  $k$ 's, associated with lower values of  $\Omega_m = 0.32 \pm 0.06$  and  $\Omega_m = 0.37 \pm 0.09$  for M3 and SFI. Figure 3 shows the likelihood as a function of  $\Omega_m$ , where for each value of  $\Omega_m$ , the nonlinear parameters obtain their most likely values. When we marginalize over the nonlinear parameters, the likelihood function is very similar. The corresponding best-fit values of  $\sigma_8 \Omega_m^{0.6}$  are  $0.49 \pm 0.06$  and  $0.63 \pm 0.08$  for M3 and SFI. These values are consistent with the estimates from cluster abundance (*e.g.*, Eke *et al.* 1998).

The reduction in the value of  $\Omega_m$  due to the nonlinear correction is similar to the mock catalog case at a relatively high degree of nonlinearity,  $r_c \simeq 0.2$  in Figure 1. The power-law segments roughly coincide with the linear  $\Lambda$ CDM segments at  $k_b$ , indicating that this broken  $P(k)$  is a sensible approximation to the actual shape of  $P(k)$ . The two catalogs basically yield consistent results. As expected, the nonlinear correction for M3 is larger than for SFI, because the former has more galaxies nearby in close pairs with small errors. The likelihood improvement for M3 is very significant,  $\Delta \ln \mathcal{L} \simeq 22$ , while for SFI it is moderate,  $\Delta \ln \mathcal{L} \sim 2.8$ .

We find that the results are quite insensitive to the choice of  $k_b$  over a wide range. At  $k_b < 0.1$ , corresponding to large pair separation and thus involving mostly distant objects of large errors, there are insufficient data to constrain the power spectrum, and the errors become big. At very large values of  $k_b$ , the analysis recovers the results of the linear analysis, but only when  $k_b$  approaches the artificial cutoff applied to  $P(k)$  arbitrarily at  $k_{\text{max}} = 8 (h^{-1} \text{Mpc})^{-1}$  for the purpose of finite numerical integration. It seems that any little freedom allowed in the model beyond the strict linear  $P(k)$  is enough for correcting the bias associated with the linear analysis. Indeed, an alternative way to incorporate nonlinear effects is by adding to the linear velocity correlation model a free parameter of uncorrelated velocity dispersion at zero lag,  $\sigma_v$ . When this correction is applied by itself, the best value of  $\Omega_m$  becomes 0.38 (instead of 0.56 in the linear analysis) with  $\sigma_v = 250 \text{ km s}^{-1}$ . When the two different nonlinear corrections are applied together, a break

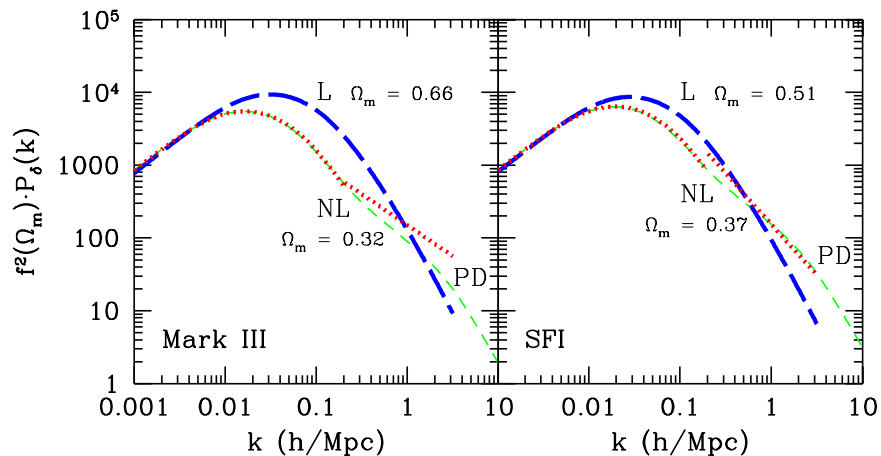


**Fig. 2.** The recovered power spectra from the real data. The  $P(k)$  yielded by the linear analysis is marked “L”, while the nonlinear analysis, with a break at  $k = 0.2 (h^{-1}\text{Mpc})^{-1}$ , is marked “NL”.

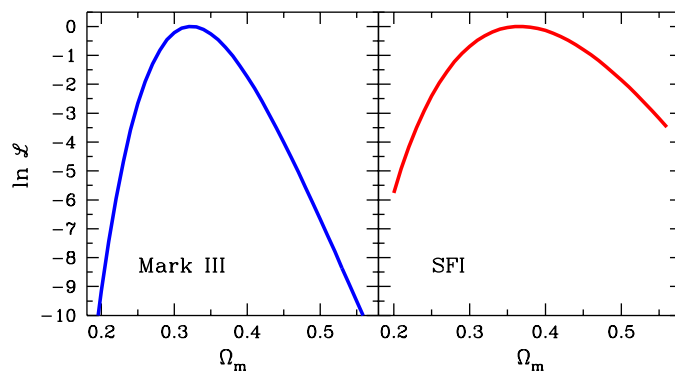


**Fig. 3.** Likelihood function for the values of  $\Omega_m$  due to the nonlinear analysis of the real data.

plus  $\sigma_v$ , the best-fit value of  $\sigma_v$  is close to zero, indicating that the two corrections are practically redundant.

## 5 Deviations from $\Lambda$ CDM

We now push the idea further, and divide the power spectrum into 4 detached segments. This allows a more general shape for  $P(k)$ , less dependent on *a priori* assumptions about a physical model such as  $\Lambda$ CDM, but at the expense of giving up the attempt to determine cosmological parameters. (The choice of a series of independent step functions, or “band powers” forming a histogram, is especially appealing computationally, because it makes the correlation

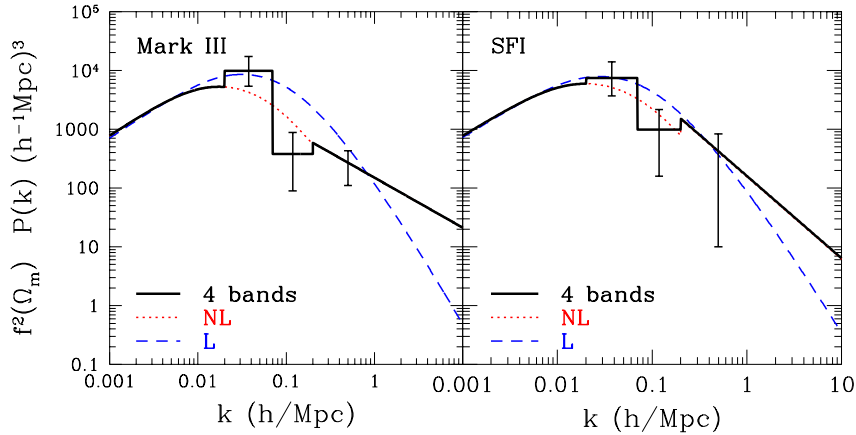


**Fig. 4.** The 4-band power spectrum of the real data, compared to the best-fit  $\Lambda$ CDM power spectra, linear (L) and nonlinear with a break (NL).

matrix a linear combination of the correlation matrices of the individual segments, and then the integrals involved need to be computed only once.) Our 5-parameter model actually consists of the following segments: (a) COBE-normalized  $\Lambda$ CDM in the extreme linear regime,  $k \leq 0.02$ , with one free parameter,  $\Omega_m$ , (b) a free constant amplitude in the interval  $0.02 < k \leq 0.07$  near  $k_{\text{peak}}$ , (c) an independent free amplitude in the interval  $0.07 < k \leq 0.2$ , and (d) a power law as before in the nonlinear regime,  $k > 0.2$ .

Figure 4 shows the recovered 4-band  $P(k)$ , in comparison with the  $\Lambda$ CDM results. The nonlinear segment practically recovers the results of the broken- $\Lambda$ CDM analysis. The two most linear segments lie along the results of the linear analysis, with a higher peak than in the broken- $\Lambda$ CDM case. The most interesting feature is the low amplitude in the interval (0.07, 0.2), in the “blue” side of the peak and just shy of the transition to the nonlinear regime. The features in the linear regime contribute only a marginal improvement to the overall likelihood, and should therefore be considered as a marginal hint only. This could be a fluke due to distance errors and cosmic variance, but the consistent appearance in the two datasets makes it intriguing.

The marginal deviation from the broken- $\Lambda$ CDM  $P(k)$  thus consists of a wiggle, with a power excess near the peak,  $k \sim 0.05$ , and a deficiency at  $k \sim 0.1$ . The missing power is reminiscent of other indications for “cold flow” in the peculiar velocity field in the local cosmological neighborhood. While the streaming motions on  $\sim 30 h^{-1}\text{Mpc}$  scales are  $\sim 500 \text{ km s}^{-1}$ , the dispersion velocity of field galaxies is only  $\sim 200 \text{ km s}^{-1}$ , indicating a high Mach number (*e.g.*, Suto, Cen & Ostriker 1992; Chiu, Ostriker & Strauss 1998; Dekel 2000).



## 6 Principal Modes: S+N versus S/N

The likelihood analysis is limited to estimating relative likelihoods for the parameters, but it does not address the absolute GOF of the model and data. The linear analysis of both M3 and SFI revealed a worry concerning the GOF, in the sense that when applied separately to two halves of the data, separated either by distance or line width, the distant data prefer a lower  $\Omega_m$ . The mock catalogs have not revealed a similar problem, indicating that it is caused by inadequacies of the correlation matrix, associated with either the theoretical or the error model. This motivates an attempt to evaluate GOF, hoping that the broken- $P(k)$  resolves the two-halves problem.

Assume a data vector  $\mathbf{c}$ , which is a random realization of an Gaussian distribution, with the correlation matrix  $C = \langle \mathbf{c}\mathbf{c}^\dagger \rangle$ . A global GOF could be evaluated using the  $\chi^2$  statistic,  $\chi^2 = \mathbf{c}^\dagger C^{-1} \mathbf{c}$ . If  $C$  is the true correlation matrix, then this value should obey a  $\chi^2$  distribution with  $n$  degrees of freedom. But this single number cannot capture all the particulars of the fitting process. A PCA, in which the data are represented in terms of the eigenvector basis of the (assumed) correlation matrix, provides a powerful tool for identifying gross features of the data and model, and for evaluating GOF in fine detail. We diagonalize the matrix via the transformation  $\mathbf{d} = \Psi \mathbf{c}$ , into  $D = \langle \mathbf{d}\mathbf{d}^\dagger \rangle = \Psi C \Psi^\dagger$ . The likelihood analysis can be performed in terms of the new “data” points  $\mathbf{d}$ . The rows  $d_i$  of  $\Psi$  are the eigenvectors, or the principal modes, and the diagonal terms  $\lambda_i$  of  $D$  are the corresponding eigenvalues. The new variables,  $d_i/\sqrt{\lambda_i}$ , are expected to be uncorrelated unit Gaussian random variables. This property is a measure of GOF, which can be evaluated by the  $\chi^2$  statistic. If this test uncovers systematic effects, they may be associated with certain features of the data and model via a detailed investigation of the eigenmodes.

The eigenmodes are ordered by the amplitude of their eigenvalues, from large to small. The high-eigenvalue modes are assigned a higher significance, because the confidence levels in the recovered parameters inversely correlate with the squares of the eigenvalues (Tegmark, Taylor & Heavens 1997), and because perturbation analysis implies that small-eigenvalue modes are more sensitive to perturbations in the correlation matrix. Since our correlation matrix is expected to be only an approximation, it would be advantageous to avoid these modes. A straightforward application of PCA is with the standard correlation matrix,  $C = S + N$ , where large eigenvalues may correspond to large signal or large noise or both. Another possibility, which we term  $S/N$ , is to first perform a “whitening” transformation,  $\mathbf{d} = N^{-\frac{1}{2}} \mathbf{c}$  (Vogeley & Szalay 1996), such that the new correlation matrix is  $D = N^{-\frac{1}{2}} S N^{-\frac{1}{2}} + I$ ,

The eigenmodes can help us identify certain features of the data and models. For example, the distance associated with a mode may be useful because distant modes are typically noisier and because it may connect to the two-halves problem. For eigenvector  $v$ , the average distance is  $\langle r \rangle_v = \sum_g |v(g)|^2 r(g)$ , where the sum is over the sample of galaxies,  $r(g)$  is the

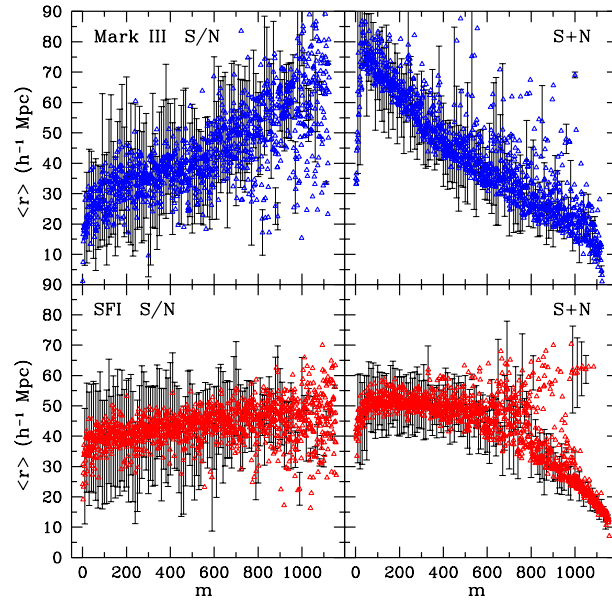


**Fig. 5.** Average distances associated with the eigenmodes of the linear  $\Lambda$ CDM model. The eigenmodes are ranked by decreasing eigenvalues (low  $m$  — high eigenvalue). The standard deviation is shown for every 10th mode.

distance of galaxy  $g$ , and  $v(g)$  defines the vector  $v$  in the basis  $g$ . If the standard deviation, defined in analogy, is small compared to the average distance, then most of the information associated with this mode comes from galaxies within a certain distance range. Figure 5 shows the average distance for each mode. The robust high S/N modes are typically associated with nearby data, which are of smaller errors. These tend to involve close pairs, and therefore stronger nonlinear effects, which makes the nonlinear correction a must. The S+N modes show a correlation with distance in the opposite sense, in which the high-eigenvalue modes are typically associated with large distances and therefore noisy data. This means that most of the S+N modes are dominated by the noise, which would not allow a sensible truncation by S+N modes, but should allow a more sensitive measure of GOF, referring in particular to the error model.

## 7 Goodness of Fit Mode by Mode

After PCA, we expect  $\chi_i^2 = d_i^2/\lambda_i$  to be about unity for each mode separately. This tests whether the eigenmodes of the prior correlation matrix are really uncorrelated with the proper variance, and, in the case of a poor fit for a certain mode, it can guide us to the source of the problem. The statistic shown in Figure 6, for each mode number  $m$ , is the cumulative  $\chi^2$  per degree of

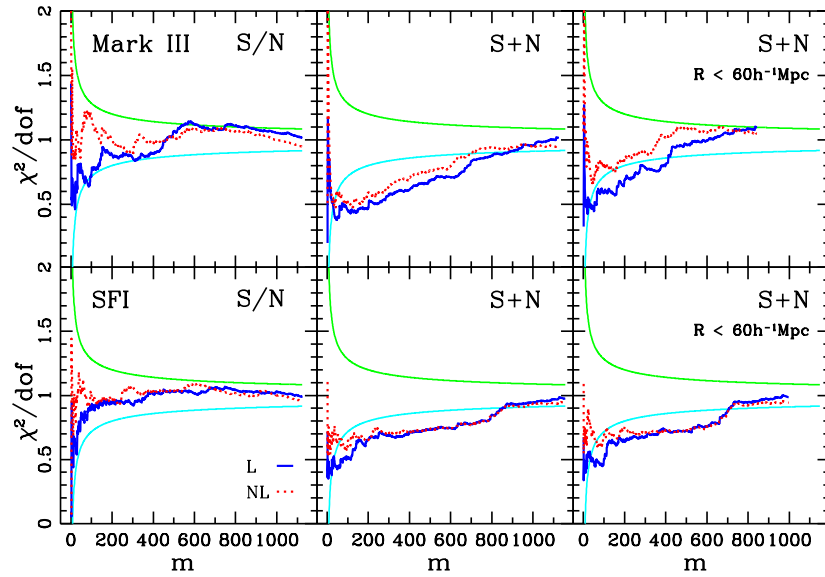


**Fig. 6.** Cummulative  $\chi^2/dof$  as a function of mode number for the linear  $\Lambda$ CDM model (solid) and for the broken- $\Lambda$ CDM  $P(k)$  (dotted). The two smooth lines mark the expected  $2\sigma$  deviations.

freedom,  $\sum_{i=1}^m \chi_i^2/m$ . The expected value is unity, and the expected standard deviation is  $\sim \sqrt{2/m}$ .

For the S/N PCA of M3, the GOF of the linear model is marginal, in the sense that the typical deviations are at the  $2\sigma$  level. The low- $m$  modes, except for the very first ones, typically have low  $\chi^2/dof$  values, while the large- $m$  modes have high values. This behavior can be translated to a systematic trend with distance via the correlation between distance and mode (Figure 5). It is therefore a reminiscence of the two-halves problem. We see in Figure 6 that the broken- $\Lambda$ CDM model clearly improves the GOF as far as the S/N modes of M3 are concerned, where the cumulative  $\chi^2/dof$  lies well inside the  $2\sigma$  contours for all the modes, with no apparent systematic dependence on  $m$ . It implies that the broken- $\Lambda$ CDM  $P(k)$  is a more appropriate model for the data.

When we analyze the S+N modes in a similar way in Figure 6, the linear model, for both data sets, shows a more severe deviation of  $\chi^2/dof$  from unity, at the  $4-5\sigma$  level, and a similar systematic dependence on  $m$ . The two-halves problem is very obvious here, with the more distant, noisy data favoring a smaller amplitude for  $P(k)$ . In this case, the use of the better, broken- $\Lambda$ CDM model makes only a small improvement which does not resolve the problem. This is a clear indication that something may be wrong in the error model as well.

We recall that the low- $m$  S+N modes are associated with large distances, where the errors are large and are known to a lesser accuracy. Guided by Figure 5, we try a poor-man compression of the data by eliminating all the data points that lie at  $> 60 h^{-1}\text{Mpc}$ . This leaves us with 843 out of the 1124 (grouped) data points of M3, and 996 out of the 1156 galaxies of SFI. This truncation causes an increase in the best-fit value of  $\Omega_m$  by less than 3%, both for M3 and SFI, and causes only a minor widening of the likelihood contours. In the case of M3, we see in Figure 6 that the S+N modes of the linear model and the truncated data show an improved GOF compared to the case of the whole data, but the  $\chi^2/dof$  still show  $\sim 3\sigma$  deviations from unity and a systematic dependence on  $m$ . However, the S+N modes of the broken- $\Lambda$ CDM model and M3 data now do lie within the  $2\sigma$  contours. The systematic trend with  $m$  is still apparent, indicating that the correlation matrix is still not perfect; either the error model is still only an approximation even for the truncated data, or the broken- $\Lambda$ CDM  $P(k)$  is not yet a perfect model (as seen in §5), or the signal and/or the noise are not exactly Gaussian, or all of the above.

In the case of SFI, while the S/N modes look very adequate with both models, for the S+N cumulative statistic the improvements due to the nonlinear correction and the elimination of large-distance galaxies are apparently not enough for an acceptable GOF. Since the large-eigenvalue S+N modes, which dominate the cumulative statistic, are dominated by noise, the limited GOF is likely to point at further shortcomings of the error model for SFI.

## 8 Conclusion

A likelihood analysis is supposed to recover unbiased values for the free parameters of a model provided that the prior theoretical model and the error model allow accurate description of the data. We addressed here tools to recover the parameters given incomplete knowledge of these models.

Using mock catalogs based on high-resolution simulations, we realized that the likelihood analysis of PV data, based on the linear  $\Lambda$ CDM  $P(k)$ , is driven by the nonlinear part of the spectrum which is not modeled accurately, and therefore yields biased results. A broken- $\Lambda$ CDM  $P(k)$ , in which the  $k > k_b$  segment is replaced by a two-parameter power law, allows a better, independent fit in the nonlinear regime. It then frees the linear regime from nonlinear effects, and yields unbiased results for  $\Omega_m$ . The results are robust to the specific choice of  $k_b$ ; we choose  $k_b = 0.2 (h^{-1}\text{Mpc})^{-1}$ , which is where the nonlinear density  $P(k)$  is expected to start deviating from the linear  $P(k)$  by the PD approximation. The results are also robust to the exact way by which the nonlinear effects are incorporated. When we add a zero-lag velocity dispersion term to the correlation function, we obtain similar results.

When applied to the real data of M3 or SFI, for a flat  $\Lambda$ CDM model with  $n = 1$  and  $h = 0.65$ , the improved analysis yields best-fits of  $\Omega_m = 0.32 \pm 0.06$  and  $0.37 \pm 0.09$ , corresponding to  $\sigma_8 \Omega_m^{0.6} \approx 0.49 \pm 0.06$  and  $0.63 \pm 0.08$ . These are in agreement with most constraints from other data, including CMB anisotropies and cluster abundance (*e.g.*, Bahcall *et al.* 1999). Joint analysis of PVs with other data is pursued based on the linear analysis (Zehavi & Dekel 1999) and the nonlinear analysis (Bridle *et al.* 2000).

By allowing an more general shape for  $P(k)$ , with 4 detached segments, we detect a marginal deviation from the  $\Lambda$ CDM, in the form of a wiggle, with an enhanced amplitude near  $k_{\text{peak}} \sim 0.05$  and a significant depletion near  $k \sim 0.1 (h^{-1}\text{Mpc})^{-1}$ . This “cold flow” on a scale of a few tens of megaparsecs is reminiscent of similar indications from the  $P(k)$  of galaxies and clusters in redshift surveys (Baugh & Gaztañaga 1998; Landy *et al.* 1996; Einasto *et al.* 1997; Suhhonenko & Gramann 1999). Most recent is the wiggle indicated in the 2dF redshift survey. The local phenomenon of cold flow may be related to the low second peak as measured by Boomerang and Maxima in the CMB angular power spectrum on a similar scale (Boomerang, de Bernardis *et al.* 2000; Maxima, Hanany *et al.* 2000). The wiggly feature may be interpreted as a deviation from the standard cosmological mass mixture, *e.g.*, a higher baryonic content than indicated by the Deuterium abundance and Big-Bang nucleosynthesis, or a non-negligible contribution from hot dark-matter. But the excess required to produce a significant wiggle seems to violate upper limits from other data; the density of baryons is limited by He+D abundances via the theory of Big-Bang nucleosynthesis (Tytler *et al.* 2000), and the density of neutrinos is constrained by large-scale structure (*e.g.*, Ma 1999; Gawiser 2000). The possibility that this feature is a statistical fluke due to cosmic variance in the context of the  $\Lambda$ CDM model cannot be ruled out yet.

A PCA, either in S/N or S+N modes, allows a fine test of GOF, by applying a  $\chi^2$  test mode by mode. It shows that the broken- $\Lambda$ CDM model is a better fit to the data than the purely linear  $\Lambda$ CDM model. For M3, using the “whitened” S/N modes, the nonlinear correction is enough to eliminate the “two-halves” problem that troubled the linear analysis. When the S+N modes are analyzed, the correction to the theoretical model is helpful but not enough for an acceptable GOF. When the M3 data is further truncated at  $60 h^{-1}\text{Mpc}$ , eliminating distant galaxies for which the errors are large and the error model is inaccurate, the GOF becomes acceptable. For SFI, the S/N modes seem adequate, but the S+N PCA indicates that the error model is still more complex than assumed.

The PCA is a powerful tool for addressing interesting properties of the data and its relation to the theoretical and error model. In particular, we associated each mode with a distance and learned about the correlation between mode eigenvalues and distance errors. This was useful in the study of GOF and in truncating the data to deal with inaccuracies in the error model. The PCA will be extremely useful when one tries to compress the data while

keeping the optimal part for determining a specific desired parameter. This compression may be mandatory for computational reasons when the body of data is excessively large. Since the model is expected to be inaccurate or incomplete, a proper compression of the data may in fact improve the results. Such data compression using PCA in the context of cosmic flows is in progress.

## Acknowledgments

This research has been partly supported by the Israel Science Foundation grant 546/98, by the US-Israel Binational Science Foundation grant 98-00217, and by the DOE and the NASA grant NAG 5-7092 at Fermilab. We acknowledge very stimulating discussions with Yehuda Hoffman, Lloyd Knox, Saleem Zaroubi and Amos Yahil.

## References

1. Bahcall, N., Ostriker, J., Perlmutter, S., & Steinhardt, P. 1999, *Science*, 284, 1481
2. Baugh, C. M., & Gaztañaga, E., 1998, in *Proceedings: Evolution of Large Scale Structure* (astro-ph/9810184)
3. Bernardeau, F., Juszkiewicz, R., Dekel, A., & Bouchet, F., 1995, *MNRAS*, 274, 20
4. Bridle, S., Zehavi, I., Dekel, A., Lahav, O., Hobson, M. P., & Lasenby, A. N. 2000, *MNRAS*, in press
5. Bunn, E. F., & White, M. 1997, *ApJ*, 480, 6
6. Burles, S., Nollett, K. M., Truran, J. N., & Turner, M. S. 1999 *Phys. Rev. Lett.*, 82, 4176
7. Chiu, W.A., Ostriker, J.P., & Strauss, M.A. 1998, *ApJ*, 494, 479
8. de Bernardis, P., *et al.* 2000, *Nature*, 404, 955
9. Dekel, A. 2000, in *Cosmic Flows: Towards an Understanding of Large-Scale Structure*, eds. S. Courteau, M.A. Strauss, & J.A. Willick, ASP Conf. Series, in press (astro-ph/9911501)
10. Dekel, A., Eldar, A., Kolatt, T., Yahil, A., Willick, J. A., Faber, S. M., Courteau, S., Burstein, D. 1999, *ApJ*, 522, 1
11. Dekel, A. & Rees, M. J. 1994, *ApJ*, 422, L1
12. Dekel, A., & Lahav, O. 1999, *ApJ*, 520, 24
13. Einasto, J., *et al.* 1997, *Nature*, 385, 139
14. Eke, V. R., Cole, S., Frenk, C. S. & Henry, J. P. 1998, *MNRAS*, 298, 1145
15. Freudling, W., da Costa, L. N., Wegner, G. Giovanelli, R., Haynes, M. P., & Salzer, J. J. 1995, *AJ*, 110, 2
16. Freudling W., Zehavi, I., da Costa, L. N., Dekel, A., Eldar A., Giovanelli, R., Haynes, M. P., Salzer, J. J., Wegner, G., & Zaroubi, S., 1999, *ApJ*, 523
17. Gawiser, E. 2000, preprint (astro-ph/0005475)
18. Górski, K. M. 1988, *ApJ*, 332, L7
19. Groth, E. J., Juszkiewicz, R., & Ostriker, J. P. 1989, *ApJ*, 346, 558

20. Hanany, S., *et al.* 2000, ApJL, in press (astro-ph/0005123)
21. Haynes, M. P., Giovanelli, R., Chamaraux, P., da Costa, L. N., Freudling W., Salzer, J. J., & Wegner, G., 1999a, AJ, 117, 2039
22. Hoffman, Y., & Zaroubi, S. 2000, ApJ, 535, L5
23. Jenkins, A., *et al.* 1998, ApJ, 499, 20
24. Kauffmann, G., Colberg, J. M., Diaferio, A., & White, S. D. M., 1999a, MNRAS, 303, 188
25. Kauffmann, G., Colberg, J. M., Diaferio, A., & White, S. D. M., 1999b, MNRAS, 307, 529
26. Kolatt, T., Dekel, A., Ganon, G., & Willick, J. A., 1996, ApJ, 458, 419
27. Landy, S. D., Shechtman, S. A., Huan, L., Kirshner, R. P., Oemler, A. A., & Tucker, D. 1996, ApJ, 456, L1
28. Ma, C. P. 1999, in Neutrinos in Physics and Astrophysics, ed. P. Langacker (World Scientific)
29. Nusser, A., & Dekel, A. 1993, ApJ, 405, 437
30. Peacock, J. A. & Dodds, S. J., 1996, MNRAS, 280
31. Sugiyama, N., 1995, ApJ (Supp.), 100, 281
32. Suhhonenko, X., & Gramann, M. 1999, MNRAS, 303, 77
33. Suto, Y., Cen, R., & Ostriker, J.P. 1992, ApJ, 395, 1
34. Tegmark, M., Taylor, A. N., & Heavens, A. F., 1997, ApJ, 480
35. Tytler, D., Fan, X. M. & Burles, S., 1996, Nature 381, 207
36. Tytler, D., O'meara, J.M., Suzuki, N., & Lubin, D. 2000, Physica Scripta, in press (astro-ph/0001318)
37. Vogeley, M. S., & Szalay, A. S., 1996, ApJ, 465
38. White, S. D. M., Efstathiou, G., & Frenk, C. S., 1993, MNRAS, 262
39. Willick, J. A., Courteau, S., Faber, S. M., Burstein, D., Dekel, A., & Strauss, M., 1997a, ApJ (Supp.), 109
40. Willick, J. A., & Strauss, M. A. 1998, ApJ, 507, 64
41. Zaroubi S., Zehavi, I., Dekel, A., Hoffman, Y., & Kolatt, T., 1997, ApJ, 486
42. Zehavi, I., & Dekel, A. 1999, Nature, 401, 252